

# Damaged Buildings Recognition of Post-Earthquake High-Resolution Remote Sensing images based on Feature Space and Decision Tree Optimization

Chao Wang<sup>1,2,3</sup>, Xing Qiu<sup>2</sup>, \*Hui Liu<sup>4,5</sup>, Dan Li<sup>4</sup>, Kaiguang Zhao<sup>3</sup>, and Lili Wang<sup>5</sup>

<sup>1</sup> Jiangxi Province Key Laboratory of Water Information Cooperative Sensing and Intelligent Processing,

Nanchang Institute of Technology, Nanchang, China, 330099;

<sup>2</sup> Key Laboratory of Meteorological Disaster, Ministry of Education (KLME), Nanjing University of Information Science and Technology, Nanjing, China, 210044;

<sup>3</sup> College of Food, Agricultural, and Environmental Sciences, The Ohio State University, Wooster, United States, 44691;

<sup>4</sup> College of Computer and Information Engineering, Hohai University, Nanjing, China, 211100;

<sup>5</sup> Jiangxi University of Science and Technology, Ganzhou, China, 341000;

**Abstract.** Earthquake-damaged buildings recognition of the high-resolution remote sensing images has been an indispensable technical means in the post-earthquake emergency response. In view of the difficulties and constraints caused by the lack of pre-earthquake information, this article proposed a novel damaged buildings recognition of high-resolution remote sensing images based on feature space and decision tree optimization. By only using post-earthquake information, the potential building object set is extracted by combining WJSEG segmentation and a group of non-building screening rules. On this basis, an adaptive decision tree number extraction strategy based on the discrimination of classification accuracy by the curve fluctuation is applied. In addition, the spectrum, texture and geometric morphology features are selected according to the feature importance index to form symbolized sets of damaged buildings. Finally, based on the optimized random forest (RF) model, buildings are separated into three categories as undamaged building, partly damaged building and ruin. Experiments on four different datasets show that the overall accuracy all exceed 85% with the proposed method, which is significantly better than the other compared methods in both visual inspection and quantitative analysis.

**Keywords:** damaged buildings; post-earthquake; high-resolution; feature importance index; decision tree optimization;

## 1. Introduction

As a fatal disaster, earthquake often occurs with casualty and economic losses. In time and accurate recognition of earthquake-damaged buildings

after the earthquake is of great significance to the rapid assessment of the condition of the disaster, carrying out emergency rescue and post-earthquake reconstruction. Compared with traditional field investigation methods, the recognition of earthquake-damaged buildings based on remote sensing images has the advantages of rapid data acquisition and wide coverage etc., which has become one of the indispensable technical means in the emergency response after the earthquake [1].

With the continuous development of remote sensor technology, the wide application of high-resolution remote sensing images has brought more detailed spatial information that is conducive to a more detailed portrayal of the earthquake-damaged buildings [2]. In this view, earthquake-damaged buildings recognition of high-resolution remote sensing images has a great potential for development and application. The existing recognition methods of earthquake-damaged buildings that only depend on the post-earthquake images has break through its dependence on the pre-earthquake images, thus have higher feasibility in the practical application. However, there is no reference change information which can be extracted from pre-earthquake image, and meanwhile such methods need to face the more prominent phenomenon of “same-object with different spectra” and “same-spectrum with different objects” caused by the increase of the spatial resolution of remote sensing images. That is, the severe challenge of the respective intra-class variance of undamaged building damaged building and other object increases and the inter-class variance decreases. Therefore, constructing more efficient feature space to describe the details of earthquake-damaged buildings accurately, which is the premise and foundation for the recognition of earthquake-damaged buildings. At present, the features which are widely used in the recognition of earthquake-damaged buildings mainly include spectra, texture and geometric morphology [3], [4], [5]. For example, Liu et al. used Morphological Attribute Profiles (MAPs) and Local Binary Pattern (LBP) to extract the geometric and texture features of the image, and then extracted the earthquake-damaged buildings by random forest (RF) classifier [6]; Asli et al. combined with spectral, compactness and smoothness features, proposed a post-earthquake collapsed buildings recognition method [7]. Although combining different kinds of features is beneficial to the multi-dimensional description of earthquake-damaged buildings, the redundant information between different features not only increases computational complexity, but also reduces the recognition accuracy due to the conflict between different features as the evidence of damaged buildings. Therefore, multi-features screening and optimization strategy for building a refined set of features is needed. On this basis, the feature set should be combined with the appropriate classification method to obtain reliable earthquake-damaged buildings recognition results. Currently, RF is a popular integrated classifier, which is applied to the field of earthquake-damaged buildings recognition based on high-resolution remote sensing images. It has the advantages of fewer model parameters and avoiding over-fitting by using the double randomness of samples and features selection [8]. For example, Solomon et al. compared RF with other classifiers, proving the good performance of RF in post-earthquake image classification [9]. Moreover, the rational selection of the number of decision trees is a key factor to improve the performance of RF. It is difficult to obtain reliable classification results when the number of

decision trees is too small, while too large will reduce the efficiency of method implementation, especially when the decision trees exceed a certain quantity, the accuracy of classification fluctuates up and down within a certain range or even has a downward trend. Nevertheless, clear quantitative criteria for decision trees is not given in RF theory [9], and the usual manual assignment way is not only susceptible to subjective factors or fall into local optimized, but also reduces the degree of automation of the classification process.

In view of the above challenges, a damaged buildings recognition of post-earthquake high-resolution remote sensing images based on feature space and decision tree optimization is proposed, and the contributions of this study can be summarized as follows:

(1) In the pre-processing step, a candidate object set extraction strategy based on WJSEG image segmentation and a group of non-building objects screening rules is proposed. It can significantly eliminate the shadows, vegetations, and non-building artificial objects.

(2) An adaptive decision tree number extraction strategy based on the discrimination of classification accuracy by curve fluctuation is proposed. By comparing with the trial and error strategy, it can not only improve the degree of automation, but also achieve ideal classification accuracy.

(3) Based on the optimized classifier, a representative feature set for damaged building description is extracted under the guidance of feature importance index. Through the experiments, this feature set shows outstanding performance in terms of the earthquake-damaged buildings recognition in complex post-earthquake scenes.

This study includes five sections. Section 2 briefly analyzes and summarizes the research progress of earthquake-damaged buildings recognition based on high-resolution remote sensing image. Section 3 elaborates the implementation steps of the proposed method. Section 4 analyses and discusses the experimental results. The conclusion is presented in Section 5.

## **2. Related Work**

In recent years, the recognition of earthquake-damaged buildings based on high-resolution remote sensing images has become a very active research direction, such as Stanford University, the University of Trento, the University of Tokyo, Wuhan University and other research institutes, which are doing related research and achieved many results. According to the different data sources used, the existing methods of earthquake-damaged buildings recognition can be divided into two categories, including multi-temporal (pre-earthquake and post-earthquake) images method and single-temporal (post-earthquake) image method [10].

### **2.1. Damaged Buildings Recognition Based on Pre-Earthquake and Post-Earthquake Images**

This kind of methods recognize the earthquake-damaged buildings by using change detection technology with the pre-earthquake and post-earthquake images. For example, Matsuoka et al. used the difference between the backscatter coefficient and the correlation coefficient of pre-earthquake, and post-earthquake SAR images to obtain the optimized window size [11]. Based on Object Based Image Analysis (OBIA), Faming Huang et al. proposed a method of recognition and loss assessment of earthquake-damaged buildings combined with single temporal image classification and multi-temporal images change detection, which achieved overall accuracy (OA) of 93% in the experiment of IKONOS images [12]. Liu Ying et al. obtained the spectral distance of the object in different temporal images by counting the Histogram Oriented Gradient (HOG), then weighting and fusing the spectral distance and HOG features, finally, the Fuzzy *C*-Means (FCM) method is applied to recognize the earthquake-damaged buildings [4]. Roberta et al. used very high-resolution optical images and existing city maps to identify objects corresponding to buildings, using spectra, textures, and statistical features to classify, and the feasibility of mapping earthquake disaster on a single building scale was evaluated [13].

Because of the introduction of pre-earthquake image, the extracted change information can be used as a key damaged buildings feature, so it is usually possible to obtain high accuracy recognition results. Nevertheless, there are many limitations in the practical application of such methods. First, for many cities, especially developing countries, the lack of reference pre-earthquake image or pre-earthquake image is inchoate to determine whether the changes in buildings are caused by earthquake directly leads to the impracticability of such methods. In addition, the quality of change detection is also significantly affected by the quality of image data, such as radiation and imaging angle differences, etc. Finally, the high accuracy registration between the pre-earthquake and post-earthquake images is also a challenging problem [10]. The above factors seriously restrict the wide application of such methods, while the single-temporal image method has been paid more and more attention by scholars [14].

### **2.2. Damaged Buildings Recognition Based on Post-Earthquake Images**

This kind of methods can only extract features from the post-earthquake image for classification. For example, based on statistical and analytical image gradient, Ye Xin et al. proposed a method based on the local spatial distribution of gradients, and further identified the different types of earthquake-damaged buildings [15]. In recent years, more and more machine-learning based methods have been proposed [16], [17]. However, such methods deeply rely on abundant samples. Christian et al. proposed a series of methods based on Support Vector Machine (SVM) and RF, which include five steps: features extraction, features screening, outlier detection, synthetic

samples generation and supervised classification, and can estimate Seismic Building Structure Types (SBSTs) information [18]. Duarte D et al. proposed a method for recognition post-earthquake damaged buildings with images of different sensors and resolutions based on Convolutional Neural Networks (CNN) and Deep Learning (DP) [19].

With the wide application of various unmanned aerial vehicles and satellite platforms, the timeliness of acquiring high-resolution remote sensing image after the earthquake has significantly enhanced. At the same time, due to this kind of methods do not rely on the pre-earthquake images, it is more in line with the application requirements. It should be noted that the proposed method in this study also belongs to this category.

### 3. Method

The proposed method mainly includes four steps: potential building set extraction, adaptive selection of the number of decision trees, feature set optimization guided by the importance index, and image classification based on optimized RF model. The specific implementation process is shown in Fig.1:

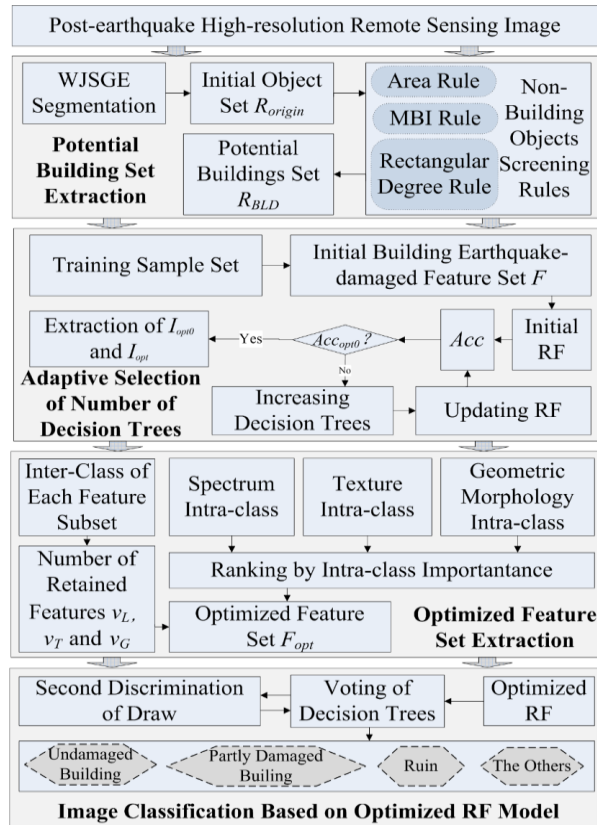


Fig. 1. Flow chart of the proposed method

### 3.1. Potential Building Set Extraction

#### ● Initial Object Set Extraction

The discrete pixels are firstly divided into geographic objects set with semantic information through image segmentation, thus providing basic analysis units for subsequent earthquake-damaged buildings recognition. For this reason, this study adopts high-resolution remote sensing image segmentation algorithm WJSEG [20], which has the following advantages: WJSEG maintains more complete outlines of geographical objects than the well-known commercial software eCognition, while helping to increase the transparency of the proposed method.

The steps of WJSEG mainly include initial seed region set conduction, secondary extraction of seed region, inter-scale constraint segmentation and regions merging. The specific implementation process of WJSEG can be found in Reference [20]. The initial object set extracted by image segmentation is represented by  $R_{origin}$  in this study.

#### ● Non-building Object Screening

Based on  $R_{origin}$ , a group of non-building object screening rules is designed in this study, thus avoiding false positives caused by such objects in subsequent processing while reducing the amount of computation. For object  $R_b$  in  $R_{origin}$ , the specific screening rules are as follows:

(1)Area rule. Count the number of pixels  $N_{pixels}$  contained in  $R_b$ . Due to the areas of buildings in remote sensing image with different resolution may have large difference, the area rule is set with experience as follows: if  $N_{pixels} \leq 80$ , then  $R_b$  is considered as the small target such as vehicles and noise, and is eliminated.

(2)Rectangular degree rule. The rectangular degree is a parameter that measures the fullness of an object and its smallest external rectangle, which can be represented as  $Rd = N_{pixels} / N_{rectangle}$  by calculating the number of pixels  $N_{pixels}$  contained in the smallest external rectangle of  $R_b$ . The aspect ratio of the smallest external rectangle of  $R_b$  is  $Ar$ . If  $R_b$  meets  $Rd < 0.8$  and  $Ar > 5$ , the object is considered to be a narrow target such as a road, river, etc., and is removed [21].

(3)Morphological Building Index (MBI) rule. MBI takes advantage of the features of pixels belonging to buildings are mostly highlighted in the gray image after top-hat transform and obtains the index value corresponding to a pixel by calculating the multi-scale differential sequence [22]. The higher the MBI, the more likely it is that the pixel belongs to a building, and the calculation formula is as follows:

$$MBI = \frac{\sum_d \sum_s DMP(d, s)}{D \times S} \quad (1)$$

where  $D$  and  $S$  represent the direction and scale of linear structural elements, respectively;  $DMP(d, s)$  is a multi-scale difference morphological sequence. According to the suggestion of document [23], this study sets  $D = 8$  and  $S = 50$ . Based on the MBI values of all pixels in the image, the

separation threshold  $T_{MBI}$  is adaptively determined by using the maximum between-class variance method (Otsu) to obtain the proportion  $Ratio_{false}$  of non-building pixels in  $R_b$ , if  $Ratio_{false} > 0.8$ , and it is removed.

According to rules (1) to (3), traverse all objects in  $R_{origin}$ , and the removed non-building objects will no longer participate in subsequent analysis and discrimination. The remaining objects will form a set of potential buildings  $R_{BLD}$  for further of earthquake-damaged buildings recognition.

### 3.2. Adaptive Selection of Number of Decision Trees

The earthquake-damaged buildings recognition based on machine learning is essentially to transform the problem of target recognition into the problem of image classification through feature extraction of post-earthquake images. The RF classifier used in this study is an integrated classifier based on non-pruning decision tree. Compared with other machine learning classifiers, it has the advantages of higher precision, stronger generalization ability and fewer parameters, which has been widely used in classification research of high-resolution remote sensing images [24]. The number  $I$  of decision trees in RF is a key parameter that significantly affects the classification accuracy. Therefore, this study proposes an adaptive selection strategy of number of decision trees, which mainly includes the following five steps:

Step1: In potential building object set  $R_{BLD}$ , 20 undamaged buildings, 20 partly damaged buildings, 20 ruins, and 20 other objects are taken by artificial marking to form the training sample set  $H$ ;

Step2: Conduct the initial building earthquake-damaged feature set  $F$ . In this study, 30 common features in the field of earthquake-damaged buildings recognition including spectrum, texture and geometric morphology are selected to construct the initial building earthquake-damaged feature set  $F$  [25], [26], [27]. Among which, the spectral features include R-band mean, G-band mean, B-band mean, R-band standard deviation, G-band standard deviation, B-band standard deviation, R-band contribution rate, G-band contribution rate, B-band contribution rate, Brightness; the geometric morphological features include Area, MajorAxis Perimeter, Eccentric Orientation, MinorAxis, Range, ConvexArea, Diameter, Solidity; and the texture features include grayscale symbiotic matrix Contrast, Homogeneity, Correlation, Entropy, J-value, Roberts operator, Sobel operator, Prewitt operator, Laplacian operator, Canny operator;

Step3: Build the initial RF model with five decision trees and enter a training sample set with all features. The classification accuracy rate is defined as the ratio of the number of correctly classified samples per tree to the number of input samples. The larger the ratio, the closer the classification result is to the real situation. Calculate the classification accuracy of each

tree, and find the mean value of the correct rate of all decision trees

$$Acc_0 = \frac{1}{5} \sum_{i=1}^5 Tree_i, \text{ which } i \text{ is the serial number of the decision tree;}$$

Step4: Build a new RF model after iteratively adding decision tree with five trees as a step size. Using the same steps as Step3, the mean value of the correct rate  $Acc_n = (\sum_{i=1}^{5(n+1)} Tree_i) / [5(n+1)]$  is obtained when the iteration number is  $n \in [1, 99]$ ;

Step5: If  $Acc_n$  meets  $Acc_{n-1} < Acc_n < Acc_{n+1}$ , it is considered to be a peak in a sub-interval containing 10 decision trees, and notes  $Acc_{opt0} = Acc_n$ ;

Step6: Continue to calculate the 3 consecutive peak points after  $Acc_n$ , which are respectively  $Acc_{opt1}$ ,  $Acc_{opt2}$ ,  $Acc_{opt3}$ , and if  $Acc_{opt0}$  satisfies:

$$Acc_{opt0} \geq \arg \max \{ Acc_{opt1}, Acc_{opt2}, Acc_{opt3} \} \quad (2)$$

the iteration is stopped and the number of decision trees corresponding to  $Acc_{opt0}$  is defined as  $I_{opt0}$ . Otherwise, proceed to the next step;

Step7: Repeat Step5 and Step6 until the  $Acc_{opt0}$  meets formula (2), stop the iteration, and  $I_{opt0}$  can be extracted. If  $Acc_{opt0}$  cannot be determined within  $n \in [1, 99]$ , the number of decision trees corresponding to the obtained maximum value of  $Acc_n$  is recorded as  $I_{opt0}$ ;

Step8: Continue to compare the classification accuracy of  $I_{opt0}$  and the four neighboring trees (9 models in total) before and after, and determine the number of optimized decision trees  $I_{opt}$  finally extracted according to the maximum classification accuracy.

### 3.3. Optimized Feature Set Extraction Guided by Feature Importance Index

Based on the optimized selection of the decision tree number of RF, in order to further reduce the redundancy and evidence conflict between the features in the candidate feature set  $F$ , this study defines an important degree index of features, and then puts forward the strategy of optimizing the feature set. In a RF model with  $I_{opt0}$  decision trees, the importance of all features is firstly calculated. Secondly, the inter-class importance of spectral, texture and geometric morphology features are calculated respectively. On this basis, the intra-class importance of sub-features included in the three types of features is calculated respectively. Finally, the optimized classification feature set of earthquake-damaged buildings is obtained under the guidance of the importance. The specific steps are as follows:

Step1: Calculate the importance of all features. In the training sample set  $H$ , the unselected samples after random sampling with return constitute an out-of-bag data set (OOB). The importance of any feature  $f_i (f_i \in F, t \in [1, 30])$  to the  $i$ th decision tree is calculated by formula (3):

$$W^{(i)}(f_t) = \frac{\sum_{x_j \in \Phi_B} N(l_j = c_j^{(i)})}{|\Phi_B|} - \frac{\sum_{x_j \in \Phi_B} N(l_j = c_{j,f_t}^{(i)})}{|\Phi_B|} \quad (3)$$

where  $\Phi_B$  represents OOB sample set,  $x_j$  and  $l_j$  respectively represent any sample in the data out-of-bag and its assigned category label,  $c_j^{(i)}$  represents the category label obtained by sample  $x_j$ ,  $c_{j,f_t}^{(i)}$  denotes a category label of sample  $x_j$  obtained by replacing the value of the feature  $f_t$  with other random values,  $N$  is a counting function. After traversing all decision trees, the importance  $W(f_t) = \frac{\sum_{i=1}^{I_{opt}} W^{(i)}(f_t)}{I_{opt}}$  of feature  $f_t$  to RF classifier can be obtained;

Step2: Calculate the inter-class importance of features. Since the features in  $F$  are respectively classified into three categories of spectrum, texture and geometric morphology (hereinafter denoted by subscripts  $L$ ,  $T$  and  $G$  respectively), the inter-class importance of the three categories of features, namely spectrum, texture and geometric morphology, can be obtained by summing up the importance of each and the categories to which it belongs respectively, and are respectively recorded as  $W_L$ ,  $W_T$  and  $W_G$ . On this basis, the spectral features normalized penalty factor for inter-class redundancy is defined as  $\varpi_L = \frac{W_L}{W_L + W_T + W_G}$ . By analogy, the normalized penalty factors of inter-class redundancy for texture and geometric morphological features are  $\varpi_T$  and  $\varpi_G$  respectively;

Step3: Calculate the intra-class importance of features. According to the spectral, texture morphological feature subsets to which the 30 features belong, the intra-class importance is calculated by Step1. On this basis, the features in each feature subset are arranged from high to low according to the intra-class importance;

Step4: For each feature subset, after rounding according to the proportion of redundant normalized penalty factors, only  $v_L$ ,  $v_T$  and  $v_G$  features with relatively high importance within the class are respectively retained, thus obtained an optimized feature set  $F_{opt}$  with  $V = v_L + v_T + v_G$  features.

### 3.4. Image Classification Based on Optimized RF Model

Based on the extracted  $F_{opt}$  and  $I_{opt}$ , an optimized RF model is constructed as follows:

$$P(x) = \arg \max_c \sum_{i=1}^{I_{opt}} E(p_i(x) = c) \quad (4)$$

where  $P(x)$  represents the classification result;  $p_i(x)$  represents the classification result of a single decision tree;  $c$  means classification label,  $c \in \{\text{Undamaged Building, Partly Damaged Building, Ruin, The Others}\}$ . On this basis, voting is carried out according to the classification labels given by each decision tree, and the number of votes is taken as the standard of the final classification label of the sample. If the voting results in a draw, the distance  $Dist$  between the sample and the training samples of these categories is discriminated according to formula (5), and the category with smaller  $Dist$  is taken as the final classification result of the sample.

$$Dist = \sqrt{\frac{\sum_{v=1}^V (x_{rest(v)} - x_{train(v)})^2}{s_v^2}} \quad (5)$$

In the formula,  $x_{rest(v)}$  and  $x_{train(v)}$  are the values of the  $v$ th feature in the test sample and training sample, respectively;  $s_v^2$  is the variance of the  $v$ th feature.

## 4. Experiment and Analysis

In the experiments, four groups of post-earthquake high-resolution remote sensing images of different sensors are used. Through visual analysis and quantitative accuracy evaluation, the performance of the proposed method is verified by comparison with a variety of advanced methods.

### 4.1. Experiment Datasets

Dataset 1 and Dataset 2 are GE01 satellite remote sensing images of Yushu in Qinghai Province, China, and the acquisition time is May 6, 2010. The earthquake occurred on April 4, 2010, with the highest magnitude of 7.1. The image includes panchromatic and multispectral (blue, green, red and near infrared) bands with spatial resolutions of 0.41m and 1.65m respectively and a size of 1024×1024 pixels. Pan-sharpened RGB images with a spatial resolution of 0.41m fused by ENVI software are used in the experiment. As shown in Fig. 2 (a) and (b). Dataset 3 and Dataset 4 are QuickBird satellite remote sensing images of Wenchuan in Sichuan Province of China, and the acquisition time is June 3, 2008. The earthquake occurred on May 12, 2008, with the highest magnitude of 8.0. The image includes panchromatic and multispectral (blue, green, red and near infrared) bands with spatial resolutions of 0.6m and 2.4m respectively. Pan-sharpened RGB images with spatial resolution of 0.6m fused by ENVI software are used in the experiments, as shown in Fig. 2 (c) and (d).

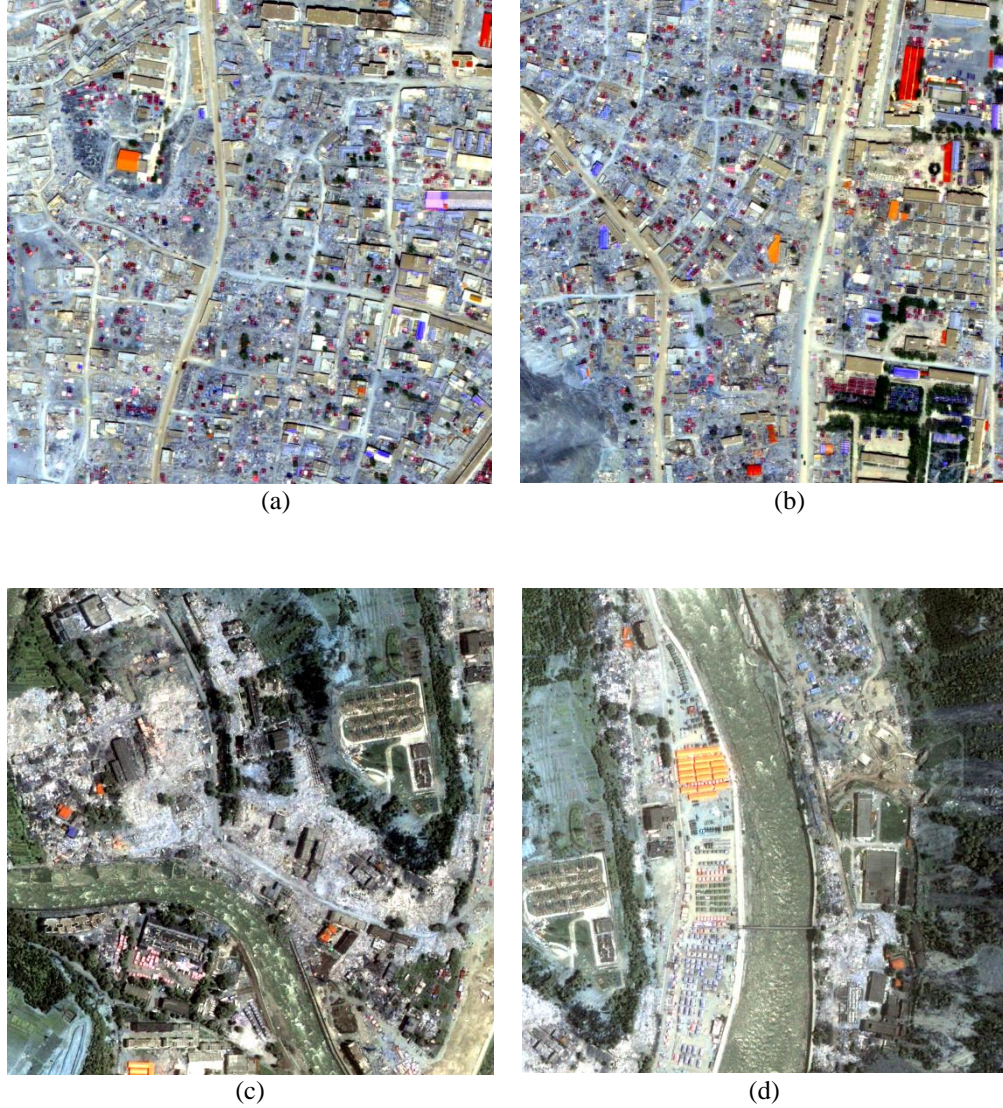


**Fig. 2.** Experimental datasets: (a) Dataset 1; (b) Dataset 2; (c) Dataset 3; (d) Dataset 4.

The reasons for selecting these four datasets for experiments are as follows: Satellite remote sensing images are one of the main forms of obtaining ground information resources at present. These datasets of different regions and sensors are selected to help analyze the general applicability of the proposed method. Besides, these areas are seriously suffered after the earthquake, including buildings, vegetations, roads, wastelands, rivers, slopes, etc. In addition, there are two types of damaged buildings, including partly damaged buildings and ruins, which is in line with the aim of the identification of damaged buildings with different degrees in this study.

## 4.2. Extraction Results of Potential Building Sets

### ● Extraction Results of Initial Object Sets

The image is firstly segmented by WJSEG method, and the initial object set  $R_{origin}$  is obtained. In order to facilitate observation, a semitransparent white layer is superimposed on the original image, and then the segmentation result is represented by black pixels and projected into the image, as shown in Fig. 3.



**Fig. 3.** WJSEG segmentation and initial object set extraction results: (a) Dataset 1; (b) Dataset 2; (c) Dataset 3; (d) Dataset 4.

It can be seen that the segmentation results have completely extracted undamaged buildings and earthquake-damaged buildings, and there is almost no phenomenon of under segmentation. The phenomenon of over-

segmentation mainly exists in river and grassland areas, which are not the region of interesting (ROI) in this study. Therefore, the extracted initial set of objects can provide effective analysis elements for subsequent earthquake-damaged buildings recognition.

● **Screening Results of Non-building Objects**

According to the discrimination rules in section 3.1, the non-building objects in initial object set are screened, and the results are shown in Fig. 4. Among them, the excluded non-building objects are represented by black pixels, and the remaining white objects constitute a potential building set  $R_{BLD}$ . At the same time, in order to facilitate analysis, some representative positions and objects in the image have been labeled with different alphabetic symbols, and the same operations are used in the following chapters.

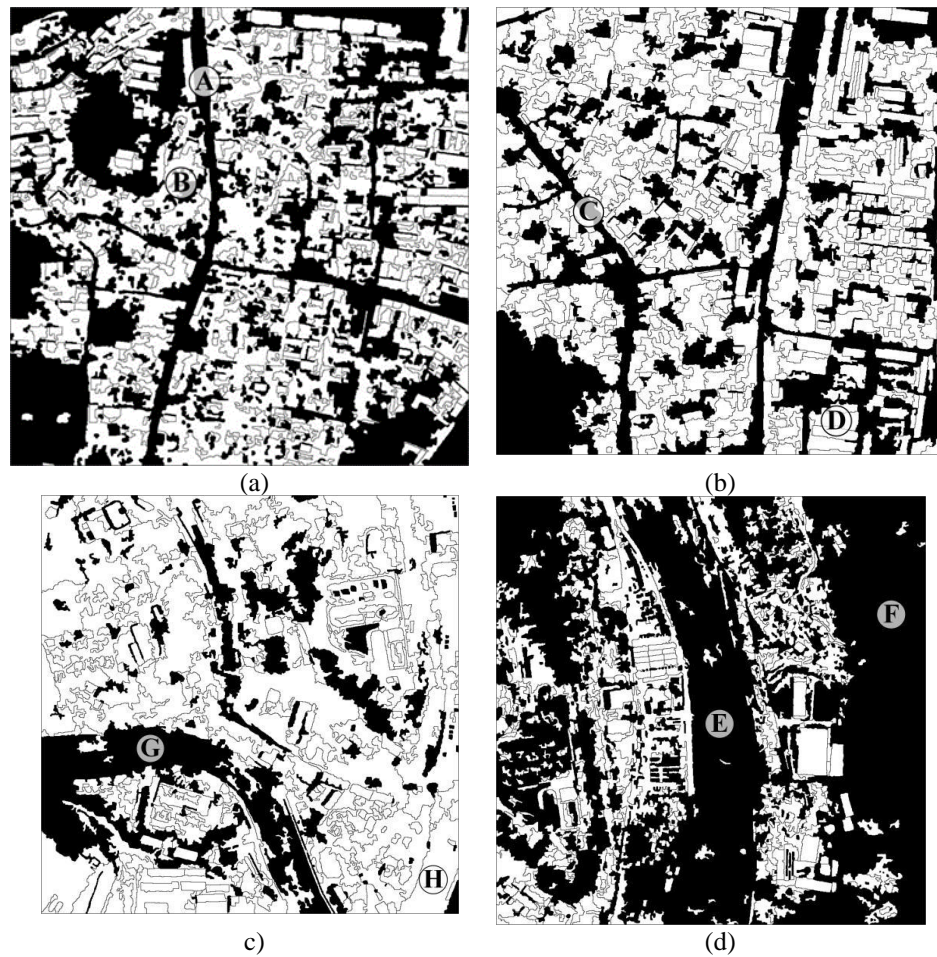


**Fig. 4.** Results of screening non-building objects: (a) Dataset 1; (b) Dataset 2; (c) Dataset 3; (d) Dataset 4.

As shown in the above figure, roads (e.g., locations A and C) in Dataset 1 and Dataset 2, tents with smaller areas (e.g., location B) in Dataset 1, river courses (e.g., locations G and E) in Dataset3 and Dataset4, and large areas of vegetation region (e.g., location F) in Dataset 4 have been effectively screened. However, there are still some non-building objects, such as wasteland (e.g., location D) in Dataset 2, Grassland and wasteland (e.g., location H) in Dataset 3. Therefore, the proposed non-building objects screening strategy is feasible and effective, but it is also necessary to retain the category of other object in the subsequent classification results.

#### 4.3. Adaptive Selection of the Number of Decision Trees

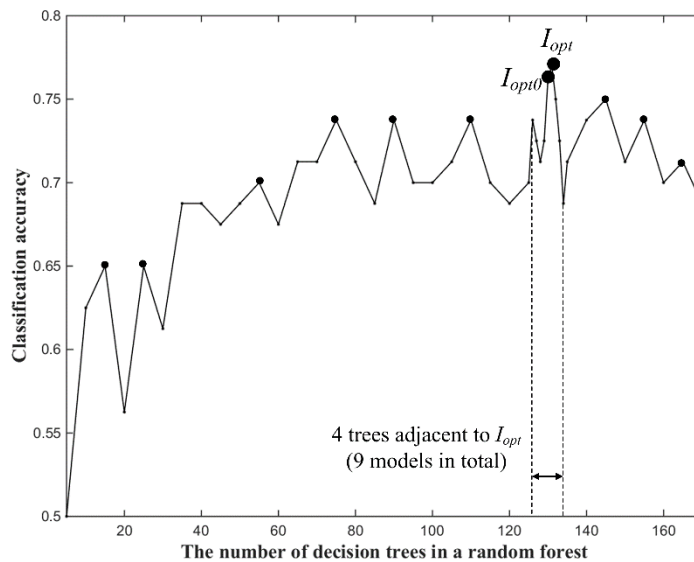


**Fig. 5.** The adaptively selected number of decision trees in Dataset 1.

The adaptively selected numbers of decision trees corresponding to Dataset 1 to Dataset 4 are 131, 64, 91 and 63 respectively. In the following, Dataset 1 is taken as an example for detailed description of adaptive selection process. As shown in Fig. 5, according to the discrimination rules in section 3.2, the satisfied condition of the selected peak point is  $I_{opt0} = 130$ . On this basis, an interval is constructed with  $I_{opt0}$  as the center, and the classification accuracy of four trees before and after  $I_{opt0}$  are calculated respectively. Among them, when the number of decision trees is 131, the classification accuracy rate reaches the maximum, so  $I_{opt} = 131$  is taken.

#### 4.4. Optimized Feature Set Extraction Results

On the basis of the adaptive number of decision trees, the optimized feature set extraction results corresponding to four Datasets are shown in Table 1 respectively:

**Table 1.** Optimized feature set extraction results

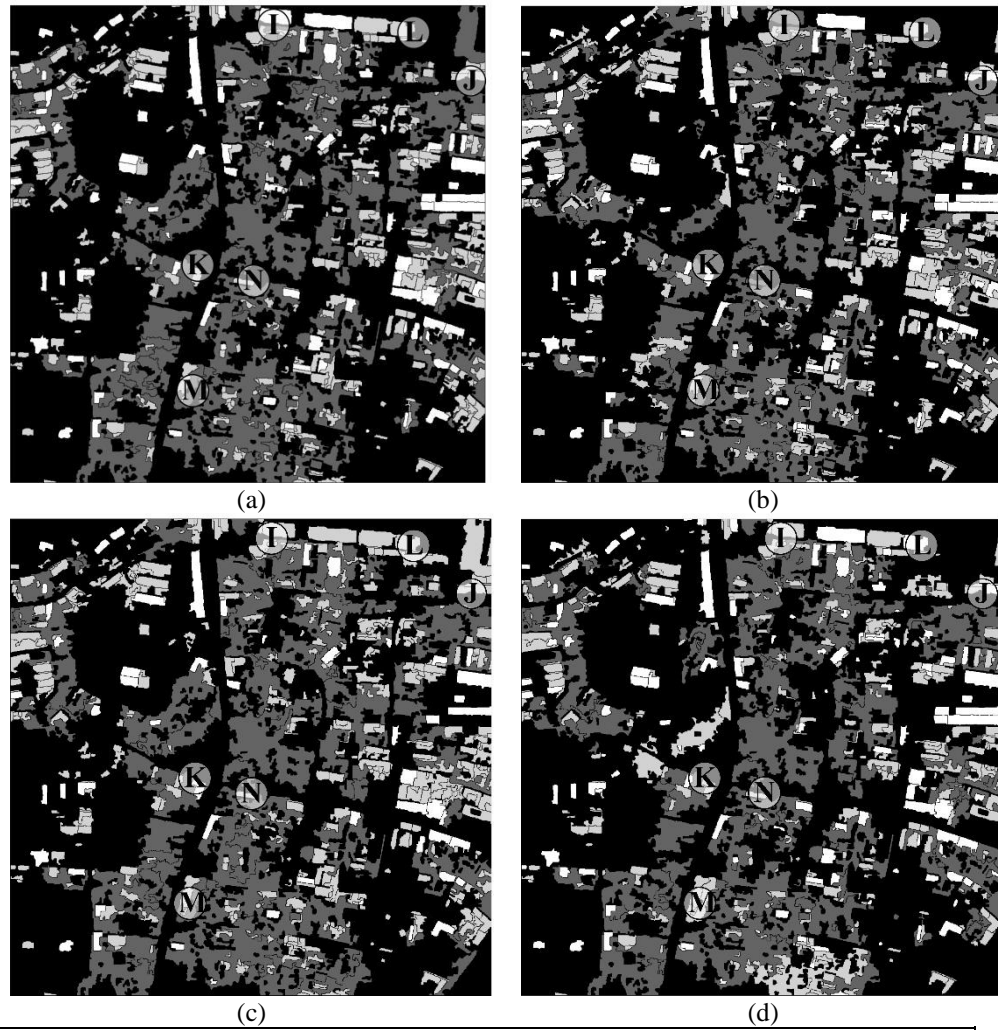
Experimental dataset	Optimized feature set
Dataset 1	G-band standard deviation, B-band standard deviation, R-band contribution rate, MinorAxisLength, Extent, Solidity, GLCM homogeneity, GCLM correlation, GLCM energy, Laplacian operator
Dataset 2	B-band standard deviation, R-band contribution rate, G-band contribution rate, MinorAxisLength, Extent, Perimeter, Solidity, Prewitt, Laplacian operator, Canny operator
Dataset 3	B-band mean, G-band standard deviation, R-band contribution rate, G-band contribution rate, B-band contribution rate, MinorAxisLength, Solidity, Laplacian operator, GLCM correlation, GLCM energy
Dataset 4	B band mean, R band standard deviation, R band contribution rate, G band contribution rate, B band contribution rate, Extent, Solidity, GLCM contrast, GLCM correlation, Laplacian operator

#### 4.5. Comparison Methods and Recognition Results

In order to objectively analyze and verify the performance of this method, traditional RF and another two advanced methods are chosen for comparative experiments. Method 1 [28] is based on the traditional RF. Set the initial building earthquake-damaged feature set  $F$  and 500 decision trees as the input of classifier. By comparing with Method 1, it is helpful to analyze the effectiveness of proposed optimization strategy for feature and the number of decision trees selection. Method 2 is an optimized RF based method with the 10-fold cross-validation [29]. More representative training damage samples are chosen for improving the recognition accuracy in this method. The

optimized feature set  $F_{opt}$  extracted in this study and 500 decision trees in original literature are used as the input. Method 3 is applied by improved Separability and Thresholds (SEaTH) for feature optimization, and extracting earthquake-damaged buildings based on membership degree. Comparing with the two advanced methods is helpful to objectively evaluate the OA of the proposed method [30], [31], [32]. In addition, since Method 2 is a pixel-level method and it is difficult to directly compare with the results of the object-level classification method in this study, the objects in the initial object set  $R_{origin}$  are used instead of pixels as the basic unit of subsequent

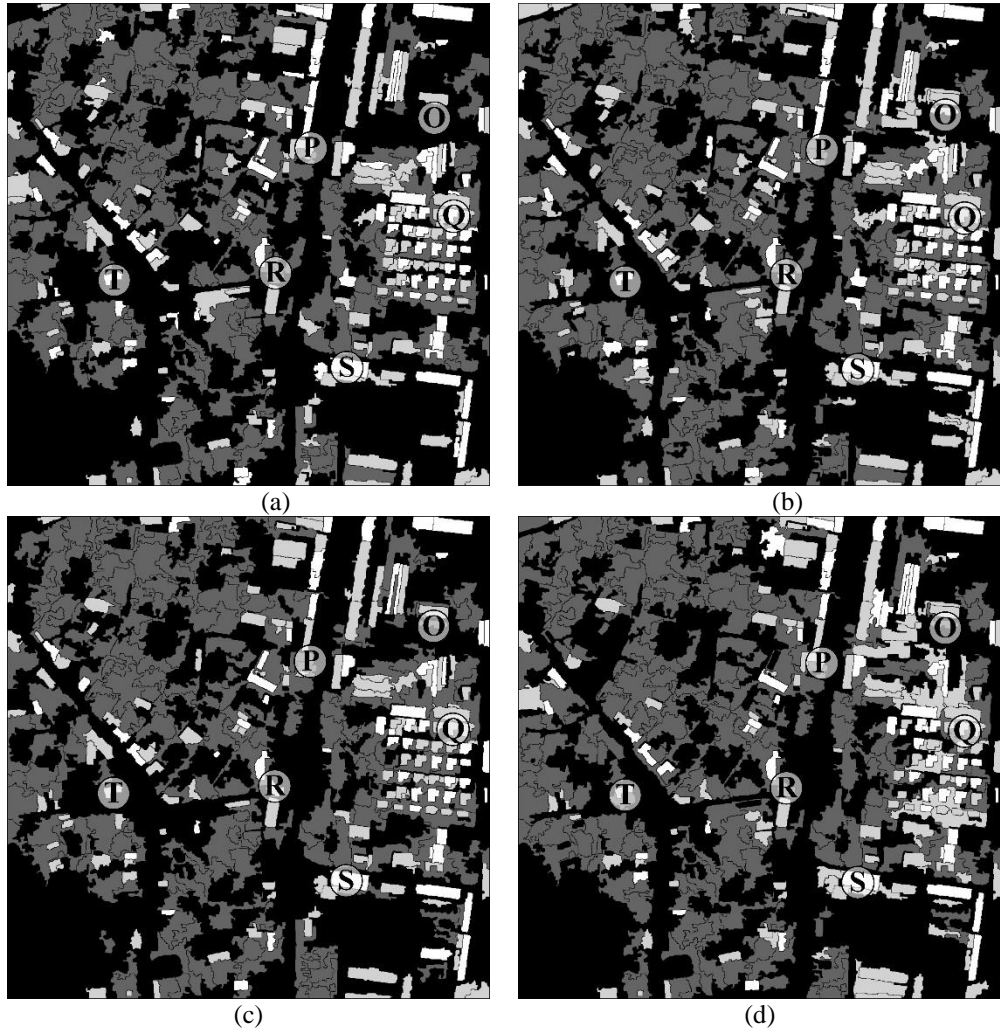
classification. Meanwhile, despite Method 3 is an object-level method, the objects in  $R_{origin}$  are also used as the basic unit for insuring the consistency of objects in classification. Besides, in order to avoid the difference in results of earthquake-damaged buildings recognition caused by whether the preliminary screening of non-buildings is taken, all the comparison methods carry out feature extraction and classification on the basis of the potential building set  $R_{BLD}$ .



Undamaged Building	Partly Damaged Building	Ruin	The Others

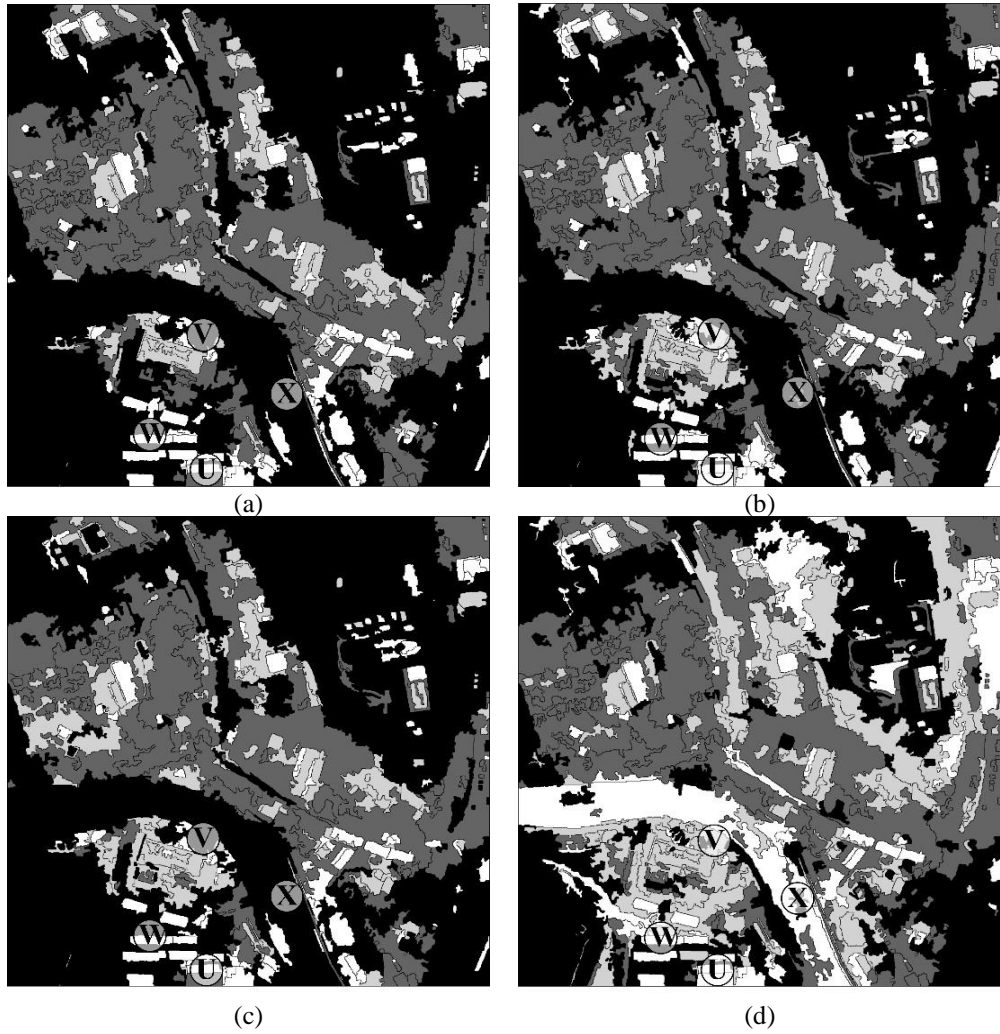
**Fig. 6.** Recognition Results in Dataset 1: (a) Method of this study; (b) Method 1; (c) Method 2; (d) Method 3.

The results of classification of all comparison methods are including four categories: undamaged building, partly damaged building, ruin and other object, which are respectively represented in different colors. The results of proposed method and three comparison methods are shown in Fig. 6 to Fig. 9.



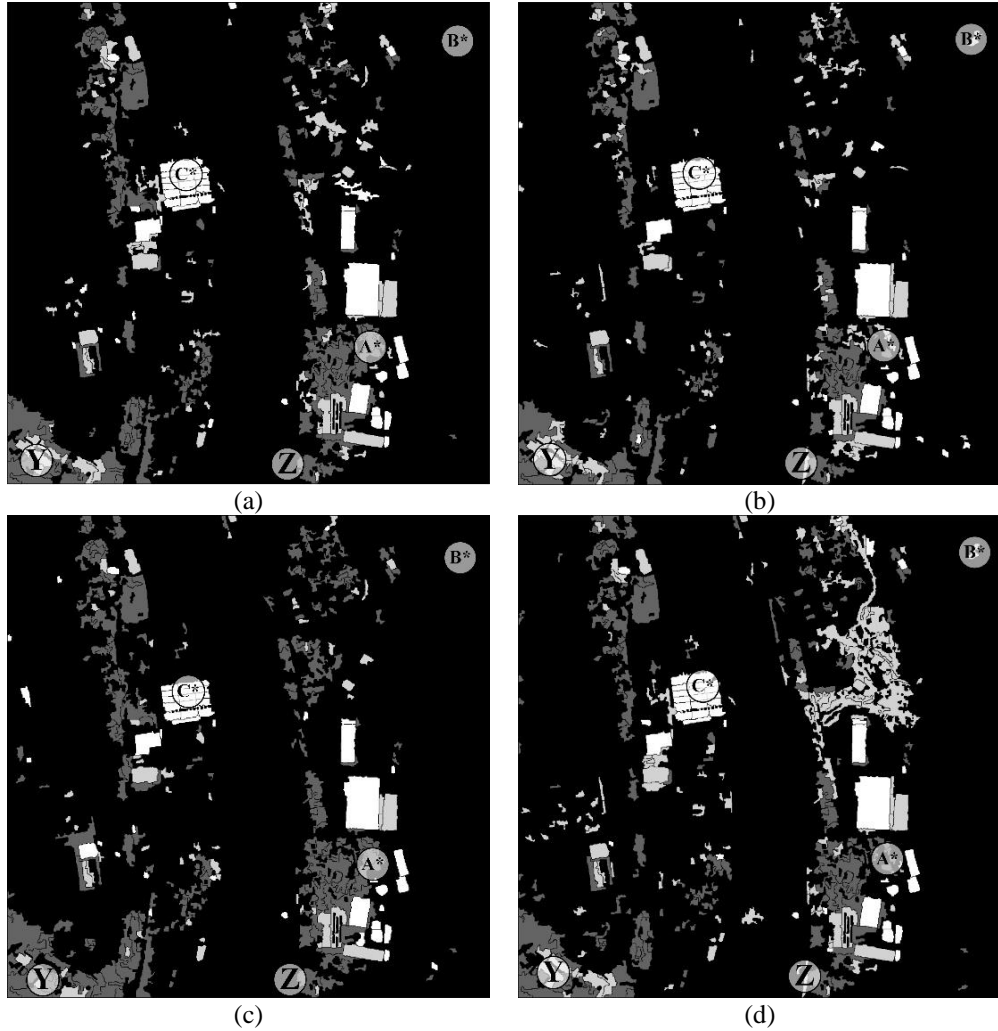
Undamaged Building	Partly Damaged Building	Ruin	The Others

Fig. 7. Recognition Results in Dataset 2: (a) Method of this study; (b) Method 1; (c)



Undamaged Building	Partly Damaged Building	Ruin	The Others

**Fig. 8.** Recognition Results in Dataset 3: (a) Method of this study; (b) Method 1; (c) Method 2; (d) Method 3

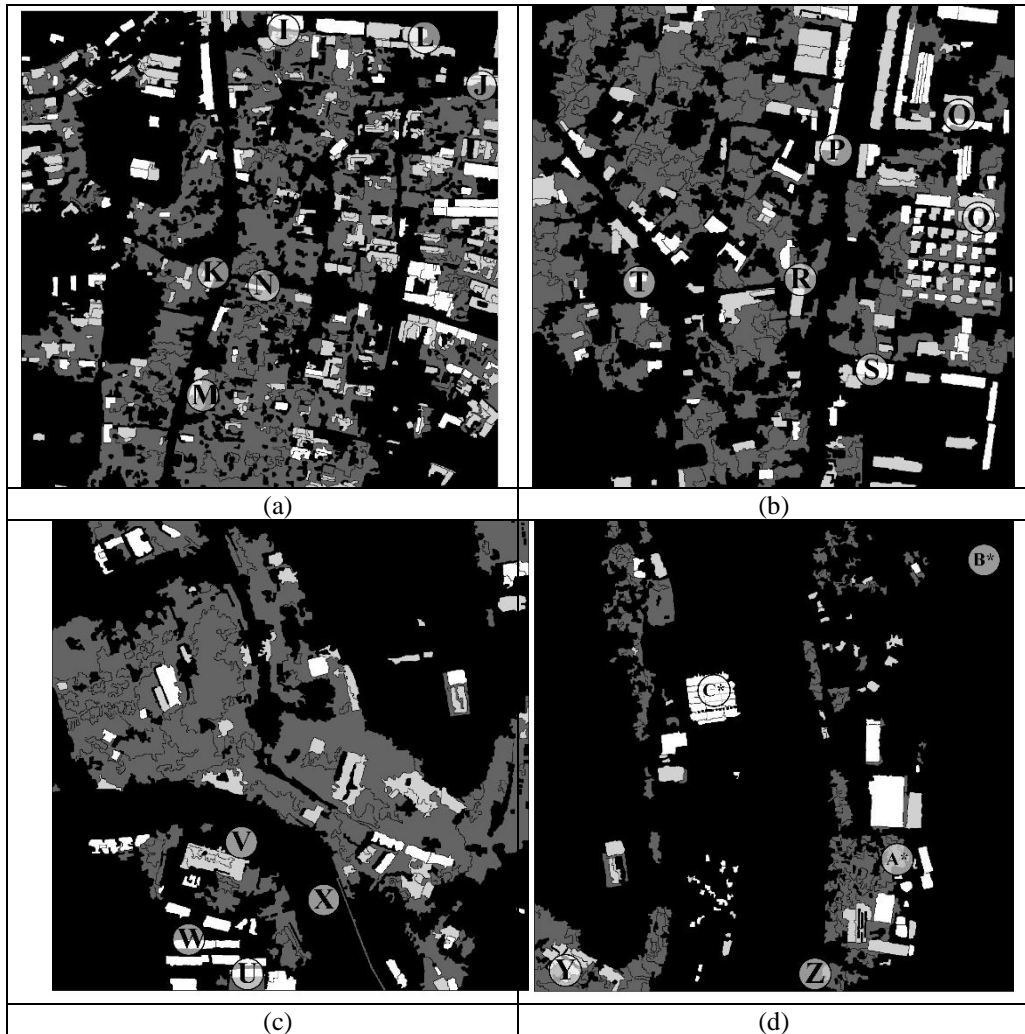


Undamaged Building	Partly Damaged Building	Ruin	The Others

**Fig. 9.** Recognition Results in Dataset 4: (a) Method of this study; (b) Method 1; (c) Method 2; (d) Method 3.

#### 4.6. Accuracy Evaluation

As the basis of accuracy evaluation, the ground truth maps of four datasets are drawn based on visual inspection and field investigation, as shown in Fig. 10.



Undamaged Building	Partly Damaged Building	Ruin	The Others

**Fig. 10.** The ground truth maps of four datasets: (a) Dataset 1; (b) Dataset 2; (c) Dataset 3; (d) Dataset 4.

● **Visual Inspection**

By comparing the experimental results with ground truth maps, the recognition effect of the proposed method is significantly better than other three methods, which mainly reflects in: (1) In the four groups of experimental results, the undamaged buildings located at locations I and Q,

the non-buildings located at location O, and the ruin located at location R are all correctly identified only by the proposed method; (2) For the undamaged buildings with regular shape and texture, such as location S, W, Z and C\*, the four methods obtain correct discrimination results; However, for partly damaged buildings, for example, only the proposed method and Method 3 obtain the correct results in location K and P, and only the proposed method, Method 2 and Method 3 have made correct judgment for location L and J; (3) For ruins, such as location U and A, only the proposed method and Method 2 have correctly identified them; (4) For non-buildings with similar spectral and shape features to buildings that have not been screened out in potential building sets, such as location V and X, only the proposed method and Method 2 obtain correct results; For some small objects, such as B\*, Z, only the proposed method and Method 2 can make correct judgment.

● **Quantitative Analysis**

On the basis of visual inspection, four accuracy indexes including OA, false positive (FP), false negative (FN) and Kappa are used to quantitatively evaluate the accuracy, as shown in Tables 2 to 5.

**Table 2.** Quantitative accuracy evaluation in Dataset 1

<b>Methods \ Indexes</b>	<b>OA</b>	<b>FP</b>	<b>FN</b>	<b>Kappa</b>
<b>Evaluation criterion</b>	<b>The bigger the better.</b>	<b>The smaller the better.</b>	<b>The smaller the better.</b>	<b>The bigger the better.</b>
<b>Proposed method</b>	<b>91.81%</b>	<b>2.89%</b>	<b>8.19%</b>	<b>0.817</b>
<b>Method 1</b>	90.14%	3.52%	9.86%	0.779
<b>Method 2</b>	90.68%	3.31%	9.32%	0.793
<b>Method 3</b>	88.69%	4.08%	11.31%	0.746

**Table 3.** Quantitative accuracy evaluation in Dataset 2

<b>Methods \ Indexes</b>	<b>OA</b>	<b>FP</b>	<b>FN</b>	<b>Kappa</b>
<b>Evaluation criterion</b>	<b>The bigger the better.</b>	<b>The smaller the better.</b>	<b>The smaller the better.</b>	<b>The bigger the better.</b>
<b>Proposed method</b>	<b>86.16%</b>	<b>5.08%</b>	<b>13.84%</b>	<b>0.781</b>
<b>Method 1</b>	78.30%	8.45%	21.70%	0.666
<b>Method 2</b>	80.17%	7.61%	19.83%	0.689

<b>Method 3</b>	77.31%	8.91%	22.69%	0.643
-----------------	--------	-------	--------	-------

Table 4. Quantitative accuracy evaluation in Dataset 3

Methods \ Indexes	OA	FP	FN	Kappa
Evaluation criterion	The bigger the better.	The smaller the better.	The smaller the better.	The bigger the better.
<b>Proposed method</b>	<b>85.99%</b>	<b>5.15%</b>	<b>14.01%</b>	<b>0.747</b>
<b>Method 1</b>	80.74%	7.37%	19.26%	0.669
<b>Method 2</b>	81.44%	7.06%	18.56%	0.668
<b>Method 3</b>	74.78%	10.11%	25.22%	0.571

Table 5. Quantitative accuracy evaluation in Dataset 4

Methods \ Indexes	OA	FP	FN	Kappa
Evaluation criterion	The bigger the better.	The smaller the better.	The smaller the better.	The bigger the better.
<b>Proposed method</b>	<b>91.89%</b>	<b>2.86%</b>	<b>8.11%</b>	<b>0.707</b>
<b>Method 1</b>	89.88%	3.62%	10.12%	0.612
<b>Method 2</b>	89.94%	3.60%	10.06%	0.640
<b>Method 3</b>	87.72%	4.46%	12.28%	0.595

From above tables, the OAs of the proposed method can always reach more than 85%, and the four accuracy indexes are superior to the other three comparison methods, which are consistent with the visual inspection results. In the experiments of dataset 1 and dataset 4, the accuracy of the four comparison methods is significantly higher than that of the other two sets of datasets, which is mainly due to the different initial screening results of non-building objects. The specific manifestation is that the proportions of screened non-building objects in the initial set of objects  $R_{origin}$  in Dataset 1 and Dataset 4 are 67.84% and 66.6%, respectively, which is significantly higher than that in Dataset 2 (34.66%) and Dataset 3 (38.35%).

Compared with the proposed method, the theoretical reasons underlying the lower accuracy of the compared methods are as follows. Method 1 adopts the unoptimized feature space and classifier, which includes more redundant information and redundancy and evidence conflict. Method 2 adopts the same training sample set and feature space, and the difference exists primarily in the number of decision trees. It has once again proved the necessity of selecting a reasonable number of decision trees. The optimize strategy of feature space in Method 3 is only based on the inter- and intra-class distance between features, while the difference between different datasets should be

considered as introducing the feature importance index proposed in this study.

#### 4.7. Analysis of Relationship between the Number of Decision Trees and OA

In order to further analyze the influence of the number of decision trees on the OA and evaluate the rationality of the number of decision trees adaptively extracted in this study, the variation curves of the OA and the number of decision trees in the four groups of experiments are counted at intervals of 10 in the interval of [50,200], and the maximum, minimum and average of OAs obtained by statistics and the OA obtained in this study are respectively expressed by straight lines of different patterns, as shown in Fig. 11.

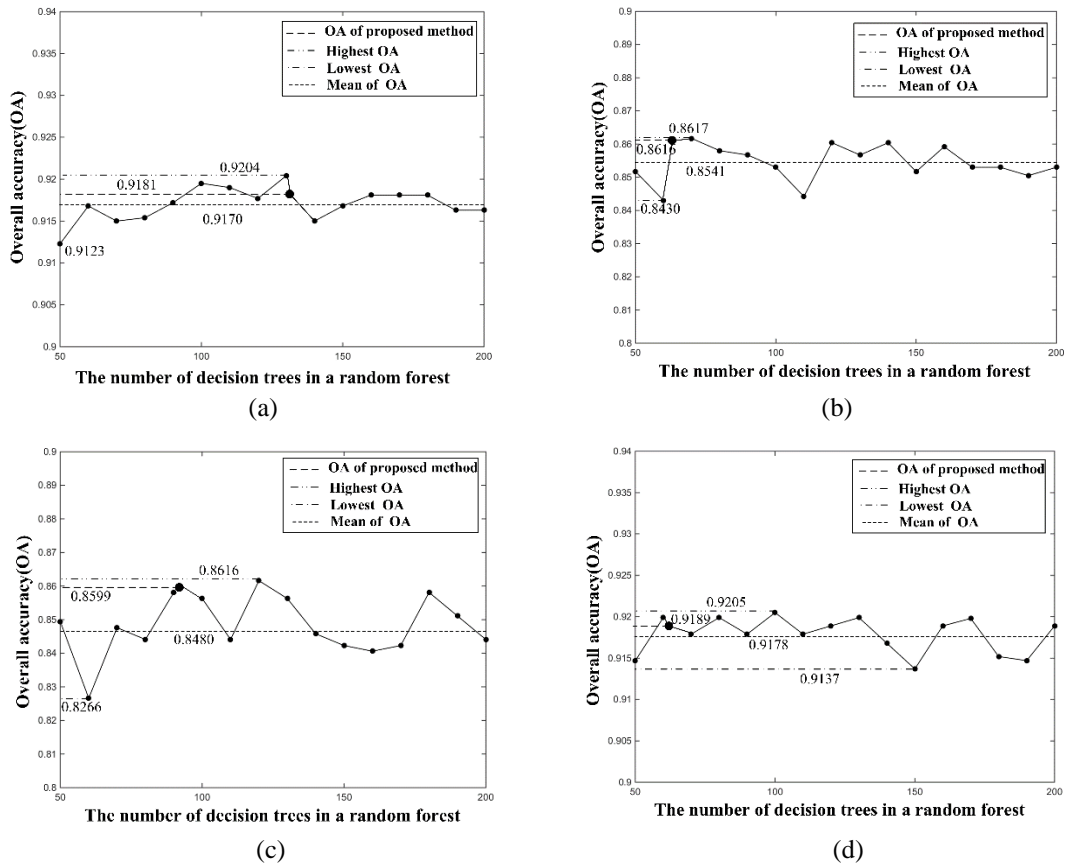


**Fig. 11.** Relationship between number of decision trees and OA: (a) Dataset 1; (b) Dataset 2; (c) Dataset 3; (d) Dataset 4.

As shown in above figures, the change in the number of decision trees has a significant impact on the OA, so it is necessary to select a reasonable

number of decision trees. On the other hand, although the OA corresponding to the number of decision trees extracted in this study is not the maximum value corresponding to the [50,200] interval, the difference is less than 1% and much higher than the average OA. Therefore, the proposed decision tree number adaptive selection strategy is feasible and effective, which not only improves the degree of automation, but also achieves ideal classification accuracy.

#### 4.8. Analysis of Influence of Feature Combination on OA

In addition to the number of decision trees, this study further analyzes the influence of different types of features and feature combinations on the detection accuracy of earthquake-damaged buildings. With the initial building earthquake-damaged feature set  $F$ , the OA obtained by statistics is shown in Table 6 according to different categories and combinations of features.

**Table 6.** Obtained OA by different features and feature combinations

<b>Features</b>	<b>OA</b>	<b>FP</b>	<b>FN</b>	<b>Kappa</b>
<b>Spectral features</b>	0.8249	0.0661	0.1751	0.6981
<b>Geometrical features</b>	0.6515	0.5856	0.8091	0.1420
<b>Texture features</b>	0.7180	0.5509	0.7863	0.1863
<b>Spectral + Geometrical + Texture features</b>	0.7723	0.4722	0.7285	0.2243
<b>The optimized features in this study</b>	<b>0.8599</b>	<b>0.0515</b>	<b>0.1401</b>	<b>0.7474</b>

As shown in the above table, the feature set extracted in this study is the corresponding to the highest OA. Besides, the OA of spectral features is significantly higher than that of the other two features when spectral, geometrical features and texture features are used alone for classification. The reason is that the inherent geometrical features and texture features of buildings are destroyed after the earthquake, which increases the uncertainty of classification. However, spectral features are not easy to change greatly, so it is more reliable in the specific application field of earthquake-damaged buildings recognition. Moreover, the OA achieved by using three types of features is even lower than that by using spectral features alone. The reason lies in feature redundancy and evidence conflict, and the feature set optimization strategy presented in this study provides an effective solution.

## 5. Conclusion

Under the premise of the lack of pre-earthquake reference information, this study proposes a method of earthquake-damaged buildings detection based on decision tree and feature optimization. In the experiments of multiple sets of high-resolution remote sensing images from different regions and different sensors, the OA can reach more than 85%, and the FN is less than 6%, which

can provide key and reliable decision support information for post-earthquake emergency response and reconstruction. Its main theoretical contributions are: (1) The proposed feature set optimization strategy guided by the important indicator of feature can provide a feasible solution for the automatic construction of feature space of earthquake-damaged buildings; (2) The proposed feature set screening strategy, combined with the adaptive extraction strategy of the number of decision trees, constructs a novel and efficient optimized RF model for earthquake-damaged buildings recognition.

**Author Contributions:** Conceptualization, C.W.; methodology, C.W. and X.Q.; software, X.Q.; validation, H.L., X.Q. and H.L.; formal analysis, X.Q. and D.L.; investigation, K.Z. and H.L.; resources, C.W.; writing-original draft preparation, X.Q.; writing-review and editing, C.W.; visualization, C.W. and X.Q.; supervision, C.W., L.W., and K.Z.; project administration, C.W.

**Funding:** This study is supported by the Open Research Fund of Jiangxi Province Key Laboratory of Water Information Cooperative Sensing and Intelligent Processing (No. 2016WICSIP004), the Six Talent-peak Project in Jiangsu Province (No. 2019-XYDXX-135), the Jiangsu Overseas Visiting Scholar Program for University Prominent Young and Middle-aged Teachers and Presidents (No. 2018-69), the National Natural Science Foundation of China (No. 61601229), the Natural Science Foundation of Jiangsu Province (No. BK20160966).

**Conflicts of Interest:** All authors have reviewed the manuscript and approved to submit to this journal. The authors declare that there is no conflict of interests regarding of the publication of this article and no “self-citations” included in our manuscript.

## References

1. Wu, J., Chen, P., Liu, Y.L.: High Resolution Remote Sensing Information Extraction Method for Earthquake Damaged Buildings. *Geography and Geo-Information Science*, Vol. 3. (2013)
2. Gan, T., Li, J.P., Li, X.Q.: Object-Oriented High-Resolution Remote Sensing Image of Building Seismic Damage Information Extraction. *Engineering of Surveying and Mapping*, Vol. 4, 11-15. (2015)
3. Ji, M., Liu, L., Du, R.: A Comparative Study of Texture and Convolutional Neural Network Features for Detecting Collapsed Buildings after Earthquakes Using Pre-Event and Post-Event Satellite Imagery. *Remote Sensing*, Vol.10, No.11, 1202. (2019)
4. Liu, Y., Li, Q.: Multi-Feature High-Resolution Remote Sensing Images for Seismic Damage Detection of Buildings. *Geomatics & Spatial Information Technology*, Vol. 6, No. 230, 71-74. (2018)

5. Li, Q., Zhang, J.F.: Study on the Identification of Damaged Buildings after Earthquake Based on the Fusion of Different Features. *Journal of Earthquake Research*, Vol. 3, 486-493. (2016)
6. Liu, Y., Cao, G.: Damage Detection Based on Multi-Feature Combination. *Computer Application*, Vol. 9, 2652-2655. (2015)
7. Sabuncu, A.: A Study of Earthquake-Induced Building Detection by Object Oriented Classification Approach. *Egu General Assembly Conference*. (2017)
8. Austin, C., Yang, S., James, C.: Detection of Urban Damage Using Remote Sensing and Machine Learning Algorithms: Revisiting the 2010 Haiti Earthquake. *Remote Sensing*, Vol. 10, 868. (2016)
9. Tesfamariam, S., Liu, Z.: Earthquake Induced Damage Classification for Reinforced Concrete Buildings. *Structural Safety*, Vol. 2, 154-164. (2010)
10. Sui, H.G., Liu, C.X., Huang, L.H., Hua, L.: Application of Remote Sensing Technology in Earthquake-Induced Building Damage Detection. *Geomatics and Information Science of WuHan Universe*, Vol. 7, 1008-1019. (2019)
11. Matsuoka, M., Yamazaki, F.: Use of Satellite SAR Intensity Imagery for Detecting Building Areas Damaged Due to Earthquakes. *Earthquake Spectra*, Vol. 3, 975-994. (2004)
12. Huang, F., Chen, L., Yin, K.: Object-Oriented Change Detection and Damage Assessment Using High-Resolution Remote Sensing Images, Tangjiao Landslide, Three Gorges Reservoir, China. *Environmental Earth Sciences*, Vol. 5, 183. (2018)
13. Anniballe, R., Noto, F., Scalia, T.: Earthquake Damage Mapping: An Overall Assessment of Ground Surveys and VHR Image Change Detection after L'Aquila 2009 earthquake. *Remote Sensing of Environment*, Vol. 210, 166-178. (2018)
14. Du, J.X.: Study and Implementation of Collapse Building Extraction Based on Morphology and Classification. *Shandong University of Science and Technology, QingDao*. (2015)
15. Ye, X., Qin, Q.M., Wang, J.: High Resolution Optical Remote Sensing Images are Used to Detect Earthquake Damage to Buildings. *Journal of Wuhan University (Information Science Edition)*, Vol. 1, 128-134. (2019)
16. Rafiei, M.H., Adeli, H.: A Novel Machine Learning-Based Algorithm to Detect Damage in High-Rise Building Structures. *The Structural Design of Tall and Special Buildings*, Vol.18, No.26, e1400. (2017)
17. Wang, N., Zhao, X., Zhao, P.: Automatic Damage Detection of Historic Masonry Buildings Based on Mobile Deep Learning. *Automation in Construction*, No.103, 53-66. (2019)
18. Estimation of seismic building structural types using multi-sensor remote sensing and machine learning techniques. *ISPRS Journal of Photogrammetry and Remote Sensing*, Vol. 104, 175-188. (2015)
19. Duarte, D., Nex, F., Kerle, N.: Satellite Image Classification of Building Damages Using Airborne and Satellite Image SAMPLES in a Deep Learning Approach. *ISPRS Annals of Photogrammetry, Remote Sensing & Spatial Information Sciences*, Vol. 2. (2018)
20. Wang, C.: A Novel Multi-Scale Segmentation Algorithm for High Resolution Remote Sensing Images Based on Wavelet Transform and Improved JSEG Algorithm. *Optik-International Journal for Light and Electron Optics*. Vol. 19, No. 125, 5588- 5595. (2014)
21. Tao, C., Tan, Y., Cai, H., Bo, D.U., Tian, J.: Object-Oriented Method of Hierarchical Urban Building Extraction from High-Resolution Remote-Sensing Imagery. *Acta Geodaetica Et Cartographica Sinica*, Vol. 39, 39-45. (2010)
22. Huang, X., Zhang, L.: A Multidirectional and Multiscale Morphological Index for Automatic Building Extraction from Multispectral GeoEye-1 Imagery. *Photogrammetric Engineering & Remote Sensing*, Vol. 7, No. 77, 721-732. (2011)

23. Fu, Q.K., Wu, B., Wang, X.Q.: Urban Building Extraction and Height Estimation Based on Morphological Building Index. *Remote Sensing Technology and Application*. (2015)
24. Rodriguezgaliano, V.F., Ghimire,: An Assessment of the Effectiveness of a Random Forest Classifier for Land-Cover Classification. *Isprs Journal of Photogrammetry & Remote Sensing*, Vol. 1, No. 67, 93-104. (2012)
25. Hongyan X., Yan Y.: Detection of Low-Flying Target under the Sea Clutter Background Based on Volterra Filter. *Complexity*, 1-12. (2018)
26. Li, Q., Jiao, Q.S.: Research on Seismic Damage Building Extraction in Beichuan County Based on Ground Lidar Technology Point Cloud. *Science Technology and Engineering*, Vol. 19, 244-249. (2016)
27. Qihao, C., Yuliang, N., Linlin, L.: Buildings Damage Assessment Using Texture Features of Polarization Decomposition Components. *Journal of Remote Sensing*. (2017)
28. Breiman, L.: Random Forest. *Machine Learning*, Vol. 1, 5-32. (2001)
29. Dou, J., Yunus, A.P., Tien, B.D.: Assessment of Advanced Random Forest and Decision Tree Algorithms for Modeling Rainfall-Induced Landslide Susceptibility in the Izu-Oshima Volcanic Island, Japan. *Science of The Total Environment*, Vol. 662, 332- 346. (2019)
30. Hongyan X., Xu Y.: Sound Source Localization Fusion Algorithm and Performance Analysis of a Three-Plane Five-Element Microphone Array. *Applied Sciences*, Vol. 9, No. 12, 2417. (2019)
31. Xu Y., Hongyan X.: Sound Source Omnidirectional Positioning Calibration Method Based on Microphone Observation Angle. *Complexity*, 1-14. (2018)
32. Wang, Z., Liu, C.: Object Level Classification of Low Altitude Remote Sensing Image Information of Unmanned Aerial Vehicle Based on SEaTH Algorithm in Lushan Earthquake. *Journal of Seismological Research*, Vol. 41, No.186, 19-25. (2018)

**Chao Wang** obtained his Ph.D. degree from Hohai University of China in 2014. He is currently an associate professor in Nanjing University of Information Science and Technology. His research interests include high-resolution remote sensing image processing and computer vision.

**Xing Qiu** is a graduate student in Nanjing University of Information Science and Technology. Her research interests include high-resolution remote sensing image processing and computer vision.

**Hui Liu** is an associate professor in Jiangxi University of Science and Technology. His research interests include high-resolution remote sensing image processing and pattern recognition.

**Dan Li** is a graduate student in Jiangxi University of Science and Technology. Her research focuses on high-resolution remote sensing image processing.

**Kaiguang Zhao** is an assistant professor of Environmental Modeling and Spatial Analysis in Ohio State University, U.S.A. His research focuses on mapping, monitoring, modeling, and managing terrestrial environments across scales, especially in the context of global environmental changes.

**Lili Wang** is a graduate student in Jiangxi University of Science and Technology. Her research focuses on high-resolution remote sensing image processing.

*Received: August 17, 2019; Accepted: January 02, 2020*